Journal of The Electrochemical Society, **159** (6) A815-A821 (2012)
0013-4651/2012/159(6)/A815/7/$28.00 © The Electrochemical Society

Dislocation Based Stress Developments in Lithium-Ion Batteries

Hsiao-Ying Shadow Huang[z] and Yi-Xu Wang

Mechanical and Aerospace Engineering Department, North Carolina State University, Raleigh, North Carolina 27695, USA

It has been suggested that structural failures are the primary factor responsible for the observed rate-capacity fade of lithium-ion batteries. In the present study, we report three different lithium intercalation-induced dislocation mechanisms explaining experimentally observed cracks. We use the theory of elasticity and the superposition method to investigate stress and force fields between multiple dislocations. In most cases, dislocations are not perfectly parallel to one specific axis. Therefore, stress variations for arbitrary Burger's vectors are investigated. The stress fields manifesting between dislocations are numerically calculated and anisotropic material properties of electrodes are employed. The result shows that multiple dislocations are likely to be orthogonal to each other to reduce the total energy. In addition, studies have shown that when the discharging rate is increased, the capacity decreases due to the buildup of the internal elastic/plastic energy. Therefore, the stress fields of dislocation interactions in our study could be used to deduce and suggest the most feasible modes of crack formation and to provide insights into the lost of capacity in $LiFePO_4$. Thus, the current study provide links between stress fields and the observed structural failure in lithium-ion batteries.
 [DOI: 10.1149/2.090206jes]

Manuscript submitted October 26, 2011; revised manuscript received March 27, 2012. Published April 10, 2012.

The potential for reduced cost, improved safety, and lowered greenhouse gas emissions by using lithium-iron-phosphate ($LiFePO_4$) as a cathode material in rechargeable battery electrodes was quickly appreciated after the first journal publication describing the use of olivine compounds.[1] Interest in high-power applications grew rapidly after Chung et al.[2] demonstrated high rate-capacity in doped nanoscale $LiFePO_4$ at room temperature,[3] but it also generated controversy about the origin of the exceptional rate performance.[4–6] $LiFePO_4$ battery chemistry promises to be an alternative to conventional lithium-ion batteries, and has attractive performance characteristics for many potential large-scale engineering applications, such as future transportation modalities and storage systems for renewable energy.[7] However, current prototype $LiFePO_4$ batteries have been reported to lose capacity over ~3000 charge/discharge cycles or to degrade rapidly under high discharging rates.[8]

It has been suggested that structural failures in cathode materials caused by lithium ion diffusion during the insertion and desertion of lithium ions are primary factors that influence the degradation of lithium-ion batteries.[9–11] Cheng and Verbrugg,[12] Zhang et al.,[13] and Christensen and Newman[14,15] have studied the diffusion-induced elastic or plastic stress developments inside electrode materials (e.g., LiS, $LiCoO_2$, $LiMn_2O_4$). Specifically, core-shell models were used in these studies to better understand energy inside particles due to lithium-ion intercalation. However, many studies have also shown that the shrinking core model is oversimplified. In particular with respect to explaining lithium-ion intercalations in plate-like nanoparticles, in which stripe-like juxtaposed phase boundaries have been experimentally observed by Chen et al.,[16] Laffont et al.,[17] and Ramana et al.[18] and computationally predicted by Cogswell and Bazant,[19] Bai et al.,[20] and Van der Ven et al.[21] Thus, to remedy the rate-capacity problems of $LiFePO_4$ batteries and cells, a rigorous analysis of mechanical-structural-electrochemical coupling is necessary.

It has been recognized that plasticity manifests in association with dislocation generation, migration and interactions in different materials systems upon lithium insertion. For example, the study by Zhao et al.[22] provided a detailed description of the evolution of elastic-plastic stresses due to lithium-ion diffusion into an inelastic host, silicon. The stress values were calculated under isotropic material property assumptions for the spherical particles. Huang et al.[23] used a single SnO_2 nanowire as the material system, and observed a high density of mobile dislocations at the reaction front upon charging. They concluded that such dislocations could potentially serve as structural precursors to electrochemically driven-state amorphization. Dislocation features and cracks in $LiFePO_4$ crystals are often observed via scanning electron microscopy (SEM) or transmission electron microscopy (TEM),[16,24] where TEM electron micrographs reveal cracks along the c-direction on the a-c plane. Similar results are reported by Gabrisch et al.[24] and it is observed that the fracture surfaces are oriented parallel to the (100) and (010) planes. As for the chemical delithiation samples, a higher dislocation density than that for the electrochemically-cycled samples is observed. The result suggests that chemical delithiation samples experience higher internal stresses due to the volume misfits. Dislocations in other cathode materials, such as $LiCoO_2$, have previously been discussed[25] and characterized;[26] collectively, it has been suggested that glissile dislocations represent a possible damage mechanism during cycling.

Dislocation induced stress fields have been widely studied in many engineering alloys,[27–30] and calculations based on a single dislocation inside a plate-like $LiFePO_4$ nanoparticle (isotropic material property assumptions) have been reported.[24] However, since the olivine $LiFePO_4$ is orthorhombic, it is appropriate to consider its fully anisotropic elastic stiffness when analyzing mechanical stresses inside particles. Therefore, in the current study we investigated mechanical energy variations due to the interactions of multiple dislocations in plate-like $LiFePO_4$ nanoparticles caused by lithium ion diffusion in the b-direction (i.e., anisotropic ion transport). This is in contrast to the radial (i.e., isotropic) diffusion-induced stress formation investigated in different materials (e.g., LiS, $LiCoO_2$, $LiMn_2O_4$) and using core-shell models.[12,14,15]

In the present study, we report three different lithium intercalation-induced dislocation mechanisms that explain experimentally observed cracks[16,24] on the *ac*-plane. We use the theory of elasticity to calculate dislocation stress fields. In most cases, dislocations are not perfectly parallel to one specific axis. For example, with $Li_{0.5}FePO_4$ samples, a slight rotation around the b-direction of the two phases was observed.[16] Therefore, stress variations for arbitrary dislocation directions are investigated. In addition, multiple dislocations usually co-exist and interact with each other in the crystal, thus we also investigate stress fields and forces between multiple dislocations. $LiFePO_4$ is chosen as the model system in the current work, due to: (a) It is recognized that $LiFePO_4$ is a promising cathode material for Li-ion batteries, thus understanding stress accumulations inside this material is important for developing longer-lasting lithium-ion battery materials, and (b) $LiFePO_4$ has a 3-D matrix structure with anisotropic elastic material properties. Once we successfully build up a model system for this sophisticated material, we will then be able to provide a general mathematical framework for other lithium-ion-battery cathode materials, such as $LiCoO_2$, $LiMn_2O_4$, and $LiNiO_2$.

[z]E-mail: hshuang@ncsu.edu

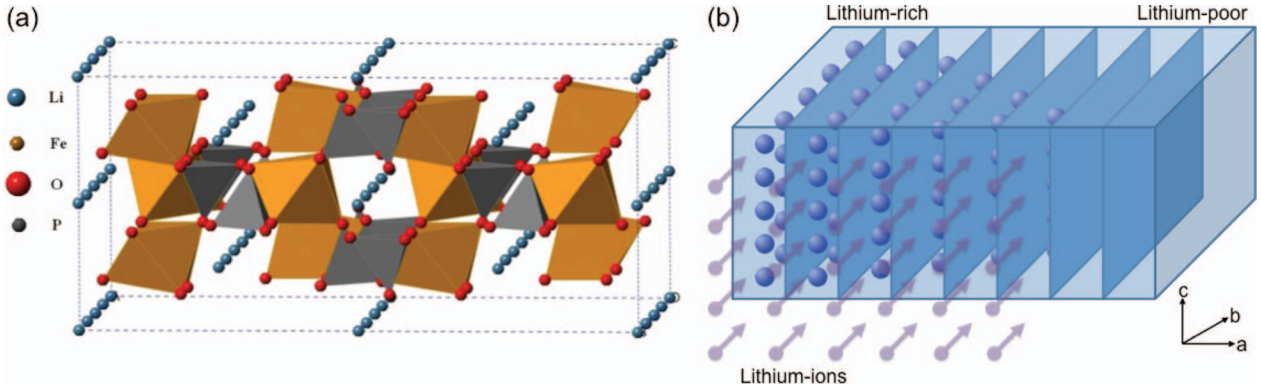

Figure 1. (a) $LiFePO_4$ crystal structure of eight unit cells. (b) During the discharging process, lithium ions intercalate into the crystal along the b-direction and fill the crystal layer by layer in the a-direction.

Lithium Ion Diffusion and Dislocation Formation

Lithium ion diffusion.— Cathode materials, such as $LiFePO_4$, typically exhibit layered structures amenable to lithium ion storage (Fig. 1a). It has been suggested that lithium ions travel in and out along tunnels in the b-direction, therefore $LiFePO_4$ crystals are filled with lithium ions layer by layer (Fig. 1b).[16,31] During repetitive and fast lithium intercalations, one or two layers in $LiFePO_4$ might be only partially-filled or skipped entirely. In this case, the crystal would then be filled with more lithium ions at one end than the other, thus generating extra-half planes with mixed edge and screw dislocations.

Dislocation formation.— From published experimental observations, fractures have been observed to be parallel to the c-direction, (001).[16,24] In the present study, we consider three possible dislocation distributions caused by coupled mechanics-structure-electrochemistry interactions; these distributions could all result in an observed (001) crack and the fracture surfaces are oriented parallel to the (100) or (010) planes. In this work, the glide planes of dislocations are determined by the lithium-ion diffusion direction (b-direction) and intercalation kinematics, in which the phase boundary (b-c plane) moves along the a-direction and is orthogonal to the direction of the lithium diffusion flux (surface flux, a-c plane), indicating that as lithium ion insertion (extraction) proceeds, layers of the 1-D channels are progressively filled (emptied) (Fig. 1b).

Edge dislocation based mode I fracture.— In the case of one or two layers in a $LiFePO_4$ crystal being only partially-filled during lithium intercalations, an edge dislocation with a (100) extra half-plane and a (010) glide plane occurs (Fig. 2a). During repetitive and fast lithium intercalations, the dislocations would result in a crack surface normal to (010) where a crack line is parallel to (001) (Fig. 2b). The dislocation experiences glide forces and the crystal particle experiences shear forces along the a-direction, suggesting a mode I fracture caused by the accumulated dislocations due to lithium intercalations (Fig. 2c), as observed from the experiments.[16,24]

Edge dislocation based mode II fracture.— Due to repetitive and fast lithium intercalations, a $LiFePO_4$ crystal might be filled with lithium ions inhomogeneously where the crystal has more lithium ions at one end than the other; an edge dislocation with a (010) extra half-plane and a (100) glide plane is formed (Fig. 3a). In this case, dislocations accumulate and result in a crack line parallel to (001) and a fracture surface parallel to (100) plane (Fig. 3b). The dislocation experiences glide forces and the crystal particle experiences shear forces along the b-direction, suggesting a mode II fracture caused by the accumulated dislocations (Fig. 3c), as observed from prior experimentation.[24]

Screw dislocation based mode III fracture.— Oftentimes, layers in $LiFePO_4$ might not be fully filled during lithium intercalation, and the crystal would have more lithium ions at one region than the other. A right-handed screw glides toward the left to extend the surface step in the required manner. Therefore, a screw dislocation with a [001] Burgers vector, a (100) extra half-plane, and a (100) glide plane is formed (Fig. 4a). The dislocation experiences glide forces and the crystal particle experiences shear forces along the c-direction, and the screw dislocation boundary would rotate with axis [100]. Accumulated screw dislocations would result in a crack line parallel to (001) and a fracture surface parallel to the (100) plane (Fig. 4b).

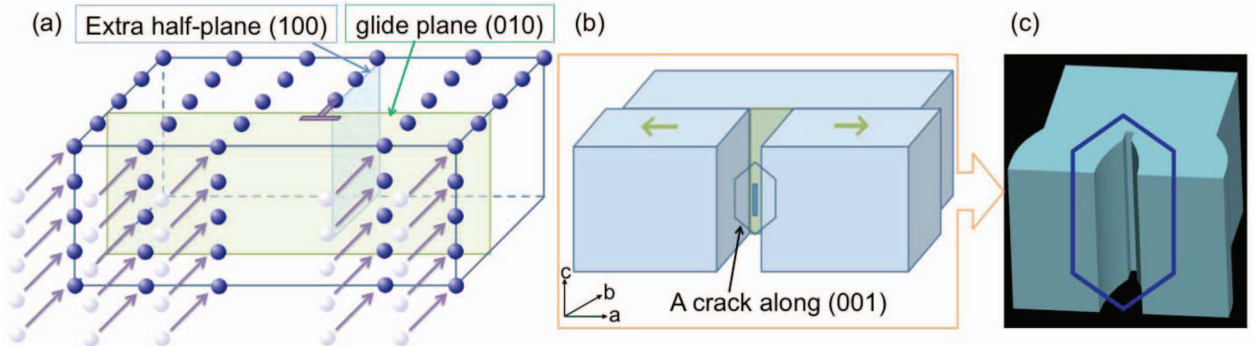

Figure 2. (a) During lithium intercalations, when one or two layers in the $LiFePO_4$ crystal are partially-filled, an edge dislocation with a (100) extra half-plane and a (010) glide plane would form. (b) With repetitive and fast lithium intercalations, the dislocations would result in a crack surface normal to (010) where a crack line is parallel to (001). (c) While experiencing shear forces along the *a*-direction, a mode I fracture caused by the accumulated dislocations would occur.

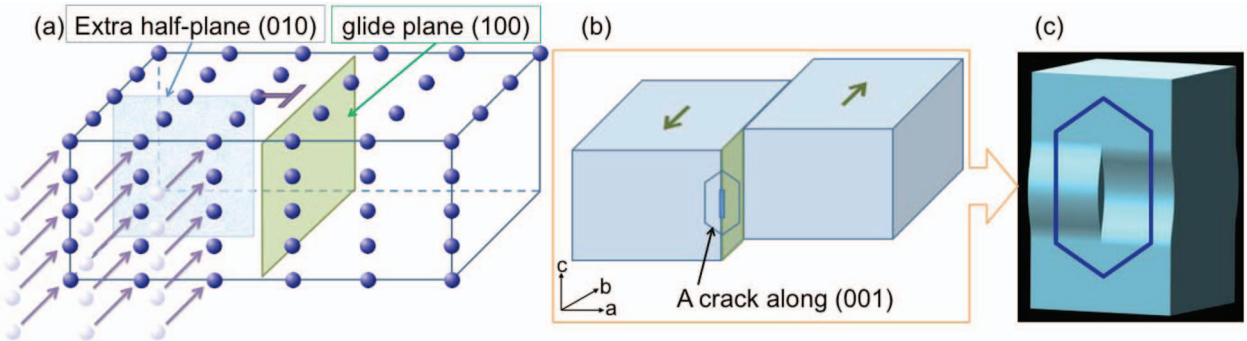

Figure 3. (a) A $LiFePO_4$ crystal might be filled with lithium ions inhomogeneously due to repetitive and fast lithium intercalations. In this case, the crystal has more lithium ions at one end than the other, and an edge dislocation with a (010) extra half-plane and a (100) glide plane would form. (b) The dislocations result in a crack surface normal to (100) and a crack line is parallel to (001), as seen from earlier experiments.[24] (c) Shear forces are along the b-direction and a mode II fracture caused by the accumulated dislocations would occur.

It is suggested that a mode III fracture is caused by the accumulated dislocations (Fig. 4c), as observed from experiments.[24]

Stress and Force Fields due to Dislocation Interactions

In the current study, we provide stress distributions of multiple dislocations in $LiFePO_4$ crystals. The directions and modes of dislocations are deduced based on experimental observations from available literatures,[16,24] as shown in Figures 2–4. Stress fields associated with edge dislocations on the *ab*-plane were calculated based on plane strain assumption,[34] and incorporating orthotropic material properties.[35] To determine the elasticity solutions for the edge dislocation, the boundary value problem were solved via a semi-inverse method by satisfying compatability equations, equilibrium equations, and displacement and traction boundary conditions.[36–38] The stress fields for one edge dislocation with arbitrary Berger's vectors are provided as follows ref 34:

in which parameters were defined as follows:

$$\bar{C}_{ij} = (C_{11}C_{22})^{1/2}, \quad \lambda = (C_{11}/C_{22})^{1/4},$$
$$\phi = \frac{1}{2}\cos^{-1}\left(\frac{C_{12}^2 + 2C_{12}C_{66} - \bar{C}_{11}^2}{2\bar{C}_{11}C_{66}}\right),$$
$$q^2 = x^2 + 2xy\,\lambda\cos\phi + y^2\lambda^2,$$
$$\text{and } t^2 = x^2 - 2xy\lambda\cos\phi + y^2\lambda^2$$

Similarly, elasticity solutions for screw dislocations on the *ab*-plane are provided in equation 2 as follows:[34]

$$\sigma_{xz} = \frac{b_z}{2\pi}\left(C_{44}C_{55} - C_{45}^2\right)^{1/2}\left(\frac{C_{45}x - C_{55}y}{C_{44}x^2 - 2C_{45}xy + C_{55}y^2}\right),$$
$$\sigma_{yz} = \frac{-b_z}{2\pi}\left(C_{44}C_{55} - C_{45}^2\right)^{1/2}\left(\frac{C_{44}x - C_{45}y}{C_{44}x^2 - 2C_{45}xy + C_{55}y^2}\right) \quad [2]$$

$$\sigma_{ij} = \frac{b_x\lambda(C_{12} - \bar{C}_{11})}{4\pi q^2 t^2 \bar{C}_{11}C_{66}\sin\phi}\left\{\begin{array}{l} C_{ij11}\left[\left(\bar{C}_{11} + C_{12} + C_{66}\right)x^2y + \lambda^2 C_{66}y^3\right] - C_{ij12}\left(\bar{C}_{11} + C_{12}\right)\left(x^3 - \lambda^2 xy^2\right) \\ -\dfrac{C_{ij22}}{C_{22}}\left[\left(\bar{C}_{11}C_{12} + C_{12}^2 + 2C_{12}C_{66} + \bar{C}_{11}C_{66}\right)x^2y - \bar{C}_{11}C_{66}\lambda^2 y^3\right] \end{array}\right\}$$
$$-\frac{b_y\lambda\left(C_{12} - \bar{C}_{11}\right)}{4\pi q^2 t^2 \bar{C}_{11}C_{66}\sin\phi}\left\{\begin{array}{l} C_{ij22}\left[\left(\bar{C}_{11} + C_{12} + C_{66}\right)\lambda^2 xy^2 + C_{66}x^3\right] - C_{ij12}\left(\bar{C}_{11} + C_{12}\right)\left(\lambda^2 y^3 - x^2 y\right) \\ -\dfrac{C_{ij11}}{C_{11}}\left[\left(\bar{C}_{11}C_{12} + C_{12}^2 + 2C_{12}C_{66} + \bar{C}_{11}C_{66}\right)\lambda^2 xy^2 - \bar{C}_{11}C_{66}x^3\right] \end{array}\right\} \quad [1]$$

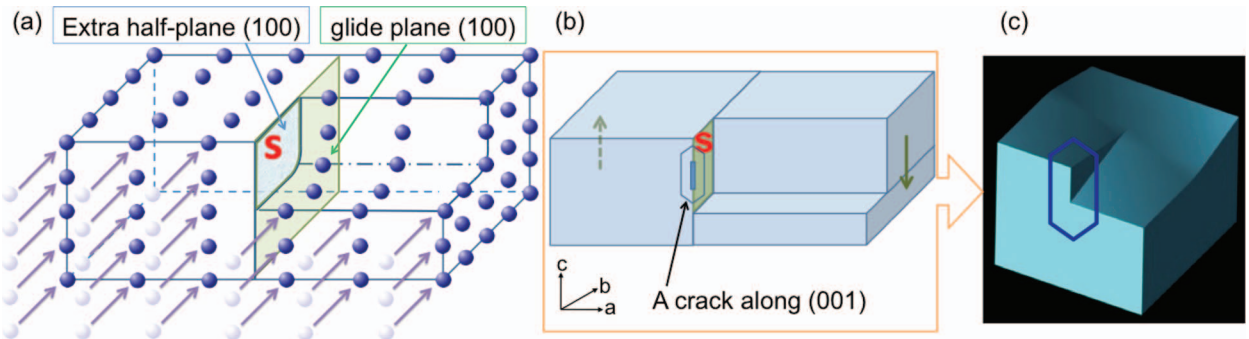

Figure 4. (a) The crystal of $LiFePO_4$ has more lithium ions at one region than the other and a right-handed screw dislocation is formed. It is with a [001] Burgers vector, a (100) extra half-plane, and a (100) glide plane. (b) The crystal particle experiences shear forces along the c-direction, and the screw dislocation would result in a crack line parallel to (001) and a fracture surface parallel to (100) plane. (c) Shear forces are along the c-direction. With accumulated dislocations, a mode III fracture would formed, as observed in prior investigations.[24]

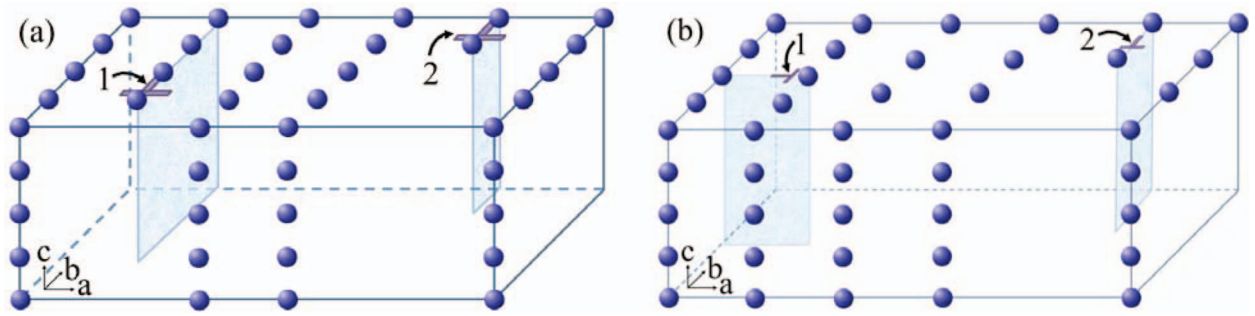

Figure 5. Representative multiple edge dislocation distributions in $LiFePO_4$ crystals. For dislocation number 1, the Burgers vectors is varied from ($b_x = 1$, $b_y = 0$) in (a) to ($b_x = 0$, $b_y = 0.6$) in (b). Dislocation number 2 is fixed in its direction.

C_{ij} (i, j = 1,..., 6) are the elastic constants for orthorhombic materials.[39] Based on the lattice parameters of $LiFePO_4$ (a = 10.334 Å, b = 6.002 Å, c = 4.695 Å),[40] the model dimensions are set as 100 L × 60 L on the *ab*-plane with 60 unit cells, where L = 10 Å. This is a plausible representative model size due to: (i) the reported $LiFePO_4$ particle size is approximately several hundred nanometers,[41] which could be correctly represented by 100 L × 60 L = 100 nm × 60 nm in the proposed model system, (ii) the model size is sufficient to avoid 4 L × 4 L dislocation core regions, the regions within which the elastic solutions would not be valid,[42] and (iii) the model size of 100 L × 60 L is sufficient to depict overall stress distributions without any boundary effects. To investigate stress variations for arbitrary dislocation directions and how dislocations interact with each other, two dislocations with different Burgers vectors were incorporated in our 100L×60L model. For dislocation number 1 (located at (x, y) = (−20 L, −12 L)), the Burgers vectors were varied among ($b_x = 1$, $b_y = 0$) (Fig. 5a), ($b_x = 1$, $b_y = 0.6$) (not shown), and ($b_x = 0$, $b_y = 0.6$) (Fig. 5b). Dislocation number 2 (located at (x, y) = (40 L, 24 L)) was fixed in its direction. The stress fields manifesting between these dislocations were numerically calculated using Mathematica (Wolfram Research, Champaign, IL). Stress fields resulting from each dislocation are calculated via Equations 1 and 2, in which the assigned locations and the superposition method[34,43] were used to obtain the overall stress distribution to better understand dislocation interactions.

When two or more dislocations are close to each other, forces of attraction or repulsion occur to reduce the total elastic energy.[44] As a result, glide or climb type motions appear in crystal structures. In the current study, we provide force fields between dislocations in $LiFePO_4$ crystals. Consider two dislocations lying parallel on a plane normal to the (001) direction, the force vector acting on dislocation 2 is expressed as: $[F] = [\sigma][b] \times [n]$, where [n] is the normal direction of the *ab*-plane, (001). The force vector is determined by the stress field [σ] of dislocation 1 and Burgers vectors [b] of dislocation 2, assuming that dislocation 1 is located at the origin (Fig. 5). For example, the forces in Figure 5a are $F_{glide} = \sigma_{xy}b$ and $F_{climb} = -\sigma_{xx}b$, where [b] = b[100] ($b_x = b$, $b_y = b_z = 0$) (Fig. 2). The forces in Figure 5b are $F_{glide} = \sigma_{yy}b$ and $F_{climb} = -\sigma_{xy}b$, where [b] = b[010] ($b_y = b$, $b_x = b_z = 0$) (Fig. 3). Equal and opposite forces act on dislocation 1 according to Newton's third law. Since we have established a comprehensive stress fields for edge dislocation 1, by varying the Burger's vector of the dislocation 2, the force field caused by these dislocation interactions is determined. The force field is numerically calculated via Mathematica and anisotropy material properties for $LiFePO_4$ are incorporated.[35]

Results

In the current study, we provide multiple dislocation stress distributions for $LiFePO_4$ crystals (Fig. 6). Representative results are shown in Figure 6 in which the dislocation 1 is located at (x, y) = (−20 L, −12 L) and the dislocation 2 is located at (x, y) = (40 L, 24 L) in our 100 L × 60 L model. Six components of stress caused by multiple dislocations with different Burgers vectors are numerically calculated. As for two edge dislocations, the stress field on the *ab*-plane is calculated by varying the Burgers vector directions of dislocation 1 when dislocation 2 is fixed in its direction: the Burgers vectors are varied from ($b_x = 1$, $b_y = 0$) in Figure 6a to ($b_x = 1$, $b_y = 0.6$) in Figure 6b to ($b_x = 0$, $b_y = 0.6$) in Figure 6c. Comparing Figure 6a to Figure 6c, it is observed that mechanical stresses between two edge dislocations could be minimized when they are orthogonal to each other, suggesting the distribution of dislocations in Figure 5b is more preferable than the one in Figure 5a. Similarly, the stress field of screw dislocation interactions is shown in Figure 6d, where the Burgers vector is $b_z = 0.47$. Moreover, the stress field for the screw dislocation is derived via the displacement in the c-direction, thus Burgers vectors in the a and b directions are unavailable (eqn 2). In general, the results reveal that the mechanical stresses are dislocation direction and location dependent. In addition, the greater the distance between two dislocations, the lower the mechanical stresses that are generated between these defects.[29] Studies have shown that when the discharging rate is increased, the capacity decreases due to the buildup of the internal elastic/plastic energy.[8,45] In this context, the results of the current study suggest that the predicted dislocation configurations (Fig. 5) could provide insight into the loss of capacity in $LiFePO_4$.

Forces of attraction or repulsion between two edge dislocations are also direction and location dependent, as shown in Figure 7. The result shows that the force field changes according to the Burgers vector direction of the dislocation 2: from $b_2 = (b_x = 1, b_y = 0)$ in Figure 7a and 7e, to $b_2 = (b_x = 1, b_y = 0.6)$ in Figure 7b and 7f, to $b_2 = (b_x = 0, b_y = 0.6)$ in Figure 7c and 7g, and to $b_2 = (b_x = -1, b_y = 0)$ in Figure 7d and 7h. Equal and opposite forces act on the dislocation 1, assuming it is located at the origin with a Burgers vector $b_1 = (b_x = 1, b_y = 0)$. Comparing between the force field in Figure 7a–7e and the ones in Figure 7c–7g and Figure 7d–7h, it is suggested that force values for arbitrary Burgers vector directions could be calculated simply by utilizing linear transformations. For two parallel edge dislocations (Fig. 7a–7e and Fig. 7d–7h), the closer they are, the stronger the attractive or repulsive forces are between them, suggesting the dislocations tend to reduce the total elastic energy by repelling each other.[29] As for two parallel edge dislocations with the same Burgers vectors (Fig. 7a–7e) or opposite Burgers vectors (Fig. 7d–7h), similar but opposite effects occur, and it is suggested that two dislocations with opposite signs tend to meet each other and cancel out the forces between them. The phenomenon shows the tendency to minimize the system energy, as observed in the case when the coherency is lost inside $LiFePO_4$ nanoparticles.[19,20] When dislocations interact, the generated force fields could be used to predict the repulsion or attraction of lithium ions in the crystal (Fig. 7). The force field studied here has been limited to the edge dislocations; however, the extension of the method to other types of dislocations is straightforward.

Discussion

Dislocations could lead to the growth of minor cracks in electrode materials after several intercalation-extraction cycles. The

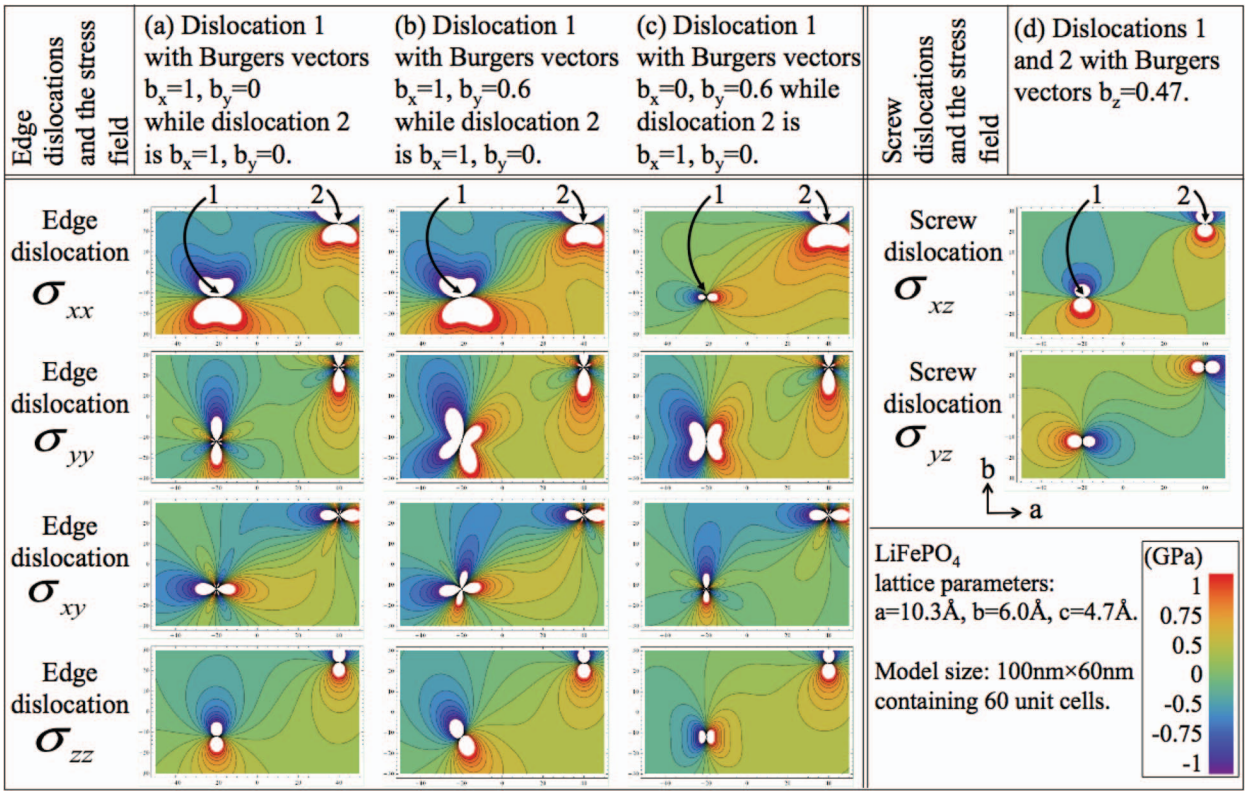

Figure 6. Stress fields for multiple edge and screw dislocations. (a) The stress field on the *ab*-plane is calculated by varying the Burgers vector directions of dislocation 1 when dislocation 2 is fixed in its direction, where the Burgers vector of dislocation 1 is ($b_x = 1$, $b_y = 0$). (b) The stress distribution between two edge dislocations for which the Burgers vector of dislocation 1 is ($b_x = 1$, $b_y = 0.6$). (c) The stress distribution between two edge dislocations for which the Burgers vector of dislocation 1 is ($b_x = 0$, $b_y = 0.6$). (d) The stress distribution between two screw dislocations for which the Burgers vector of dislocation 1 is ($b_z = 0.47$). In general, the results reveal that the mechanical stresses are dislocation direction and location dependent, and the greater the distance between two dislocations, the lower the mechanical stresses that are generated between these defects.[29] Studies have shown that when the discharging rate is increased, the capacity decreases due to the buildup of the internal elastic/plastic energy.[8,45] Therefore, the stress fields of dislocation interactions could be used to provide insights into the lost of capacity in $LiFePO_4$.

accumulation of glide will finally cause cracks and even further structural failures. Cracks in electrode materials could limit the electron/lithium ion diffusion rate and increase the impedance of lithium-ion batteries, as suggested and supported by other studies.[9–11] Moreover, cracks could create smaller particles with larger surface areas, which could increase the heat absorption and aggravate side reactions such as the dissolution of the transition metal in electrolytes.[32,33,46]

The significance of the present study is that we provide a visualization of the stress distribution resulting from multiple dislocation

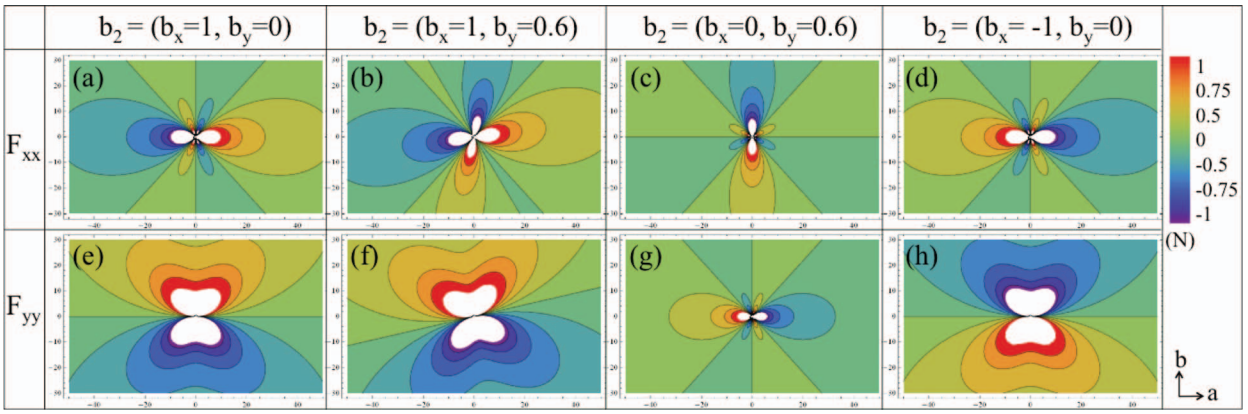

Figure 7. The force field of dislocation interactions. Forces are calculated via $[F] = [\sigma][b]\times[n]$, where [n] is the normal direction of the *ab*-plane, (001), [σ] is the stress field of dislocation 1, and [b] is the Burgers vector of dislocation 2, assuming dislocation 1 is located at the origin with a Burgers vector $b_1 = (b_x = 1, b_y = 0)$. The force field changes due to the direction of dislocation 2. (a) and (e): $b_x = 1$, $b_y = 0$; (b) and (f): $b_x = 1$, $b_y = 0.6$; (c) and (g): $b_x = 0$, $b_y = 0.6$; (d) and (h): $b_x = -1$, $b_y = 0$. Equal and opposite forces act on dislocation 1. Comparing the force field in (a)(e) with the ones in (c)(g) and (d)(h), it is suggested that force values for arbitrary Burgers vector directions could be calculated simply by utilizing linear transformations. When dislocations interact, the generated force fields could be used to predict the repulsion (red) or attraction (blue) of lithium ions in the crystal. Therefore, lithium-ions are not necessary filled in one layer before proceeding to the next layer during fast discharging, as shown in Figure 1b and Figure 5.

interactions in 60 unit cells, in which the anisotropic material properties of $LiFePO_4$ have been adopted, as in other computational models.[19,20,35,47] Since the stress field resulting from a dislocation could affect neighboring atoms, an adequate number of unit cells is required to better describe the stress distributions of the dislocations. In the current study, the model dimensions are set as 100 L × 60 L on the *ab*-plane with 60 unit cells. It is a plausible representative model size since the reported $LiFePO_4$ particle size is approximately several hundred nanometers,[41] which could be correctly represented by 100 L × 60 L = 100 nm × 60 nm in our model system. In addition, the model size is sufficient to avoid 4 L × 4 L dislocation core regions (Fig. 6), the regions within which the elastic solutions would not be valid.[42] Furthermore, the model size of 100 L × 60 L is sufficient to depict overall stress distributions without any boundary effects. In addition, by providing the stress field in at least 60 unit cells, we could also clearly understand and observe that how stresses "travel, distribute, and interact" inside electrode particles. For example, Tang's model[47] contained at least 80 unit cells and Cogswell's model[19] contained at least 500 unit cells. However, while single stress or energy values[24] provide a foundation for further simulations, they do not reveal information on how dislocation-induced stresses "travel, distribute, and interact" within $LiFePO_4$ nanoparticles.

Experimental TEM/SEM images have revealed that some dislocations are not perfectly aligned along any one particular lattice axis, as shown in Chen et al.,[16] Laffont et al.,[17] and Ramana et al.[18] Thus, in the current work, we present a model capable of capturing the variations of Berger's vector directions in multiple unit cells. In addition, the representative multiple edge dislocation distributions were deduced based on the dislocation movement reported by Gabrisch et al.[24] Oftentimes, when a dislocation/crack is identified experimentally via TEM/SEM, the only information available is its orientation.[16–18,24] Therefore, we compared different possibilities of a dislocation formation (Fig. 2, 3, and 4), based on the reported lithium-ion diffusion direction (b-direction). From the calculated lowest energy state or stress distribution, multiple dislocations are likely to be orthogonal to each other (Fig. 6c), rather than parallel to each other (Fig. 6a). Therefore, we were able to deduce and suggest the most feasible mode of fracture or multiple dislocation formations due to lithium-ion intercalation, as shown in Figure 5b.

Since $LiFePO_4$ undergoes a two-phase separation under low current,[20,48] and the solid solution is present during (dis)charging,[1,6,49–51] $LiFePO_4$ is likely thermodynamically analogous to a two-phase alloy. Nevertheless, careful examination of multiple dislocation-induced stress distributions in such two-phase $LiFePO_4$ nanoparticles have not been treated explicitly. Therefore, in the current study, we aimed to integrate a well-established method (i.e., calculation of stress fields from dislocation interactions) with an important lithium ion battery material (i.e., $LiFePO_4$) to study stress fields resulting from dislocation interactions. This approach, wherein we relied on a well-established calculation method (i.e., elastic solutions of dislocation interactions), allowed us to focus on delineating the stress distributions in $LiFePO_4$ associated with the observation of multiple dislocations.

Various lithium-ion intercalation mechanisms in $LiFePO_4$ have been proposed in different studies, and our model system (Fig. 1b) focuses on one with lithium-ion intercalation as reported by Bai et al.,[20] and Zhao et al.[52] According to these studies, lithium ions undergoing fast intercalation exhibit strongly anisotropic transport properties. By contrast, the domino-cascade model proposed by Delmas et al.[31] did not include such anisotropy; specifically, the phase-boundary of the domino-cascade model moves in the a-direction and requires lithium-ions to be filled completely layer-by-layer. Furthermore, the interface in the domino-cascade model is limited to one $FePO_4$ block, and depending on the size of the crystallites, the mismatch between the unit cells require several atomic layers in the boundary.[31] Therefore, it is suggested these misfits in multiple layers could be minimized by energy relaxation associated with the formation of dislocations or cracks.[31] Furthermore, based on the stress field of dislocation interactions, it is suffice to say that our current model containing 60 unit cells is adequate to describe phase boundary movements during lithium-ion intercalation (Fig. 6).

In addition, according to the study by Zhao et al.,[52] the distribution of lithium ions in the active particle is inhomogeneous during fast intercalation; it is unnecessary for lithium ions to be filled completely in one layer before advancing to the next layer (Fig. 1b). A layer could possibly be skipped or remain only partially filled, and different modes of dislocations can potentially result from non-homogenously distributed lithium atoms during intercalation (Fig. 5). By contrast, under low current, i.e. during slow (dis)charge, it has been suggested that coherency strain due to volume misfits reduces the critical current for homogeneous intercalation,[20] therefore a two-phase solid-solution is generally observed. However, under high current, i.e., during fast (dis)charge, it has been suggested that there are no phase boundaries where coherency strain does not play any role.[48] In the current study, the effect of crystallite boundaries was not investigated, since recent reports have shown that either a single phase[48] or stripe-like co-existent phases[19] are likely present in $LiFePO_4$ nanoparticles, suggesting that phase separation may be suppressed, as observed by Chen et al.[16]

The current study aims to provide a computational predictions and insight complementary to available experimental observations.[16,24] While quantitative stress or strain energy values are important,[24] we consider a stress distribution inside 60 unit cells of $LiFePO_4$, incorporating anisotropic materials properties and rotations of Burger's vectors, could go beyond experimental observations with a detailed mechanical description that leverages current TEM/SEM observations, and potentially provides avenues for better understand how multiple dislocations could potentially form in $LiFePO_4$ nanoparticles, as many studies have suggested that a loss of coherency could potentially be due to the formation of dislocation during fast discharging.[19]

Conclusions

Mechanical and structural failures are attributed to dislocation formations. Here, we provide analytical models of stress and force distribution generated by multiple dislocations in $LiFePO_4$ nanoparticles. We deduce that crack formations are caused by the accumulation and movement of dislocations due to lithium ion diffusion during charging or discharging. The stress and force field provide herein are useful for predicting the dislocation generations and movements and could benefit future battery development research. The important findings of the current work are as follows:

1. We report stress fields caused by multiple dislocations inside $LiFePO_4$ nanoparticles. Different dislocations with different Burgers vectors have significant influences on the stress developments. Based on the stress and force fields obtained in the current study, it is believed that fractures inside electrodes are potential failure mechanisms responsible for the rate-capacity loss in lithium-ion batteries.
2. From the experimental observations reported by Gabisch et al.[24] and Chen et al.,[16] we further confirm our hypothesized mechanisms of mode I, II, and III cracks formation from the lithium-ion diffusion and dislocation movement phenomena.

This study contributes to the fundamental understanding of the internal stress developments in lithium-ion battery electrodes. A greater understanding of the mechanisms studied here would help with designing better lithium-ion batteries, and thus advances technology in energy storage systems and leads to economic and environmental benefits.

References

1. A. K. Padhi, K. S. Nanjundaswamy, and J. B. Goodenough, *Journal of the Electrochemical Society*, **144**, 1188 (1997).
2. S.-Y. Chung, J. T. Bloking, and Y.-M. Chiang, *Nature Materials*, **1**, 128 (2002).
3. S. Y. Chung, J. T. Bloking, and Y. M. Chiang, *Nature Materials*, **2**, 702 (2003).
4. N. Ravet, A. Abouimrane, and M. Armand, *Nature Materials*, **2**, 702 (2003).

5. K. Striebel, J. Shim, V. Srinivasan, and J. Newman, *Journal of the Electrochemical Society*, **152**, A664 (2005).
6. C. Delacourt, P. Poizot, J.-M. Tarascon, and C. Masquelier, *Nature Materials*, **4**, 260 (2005).
7. Y.-M. Chiang, *Science*, **330**, 1485 (2010).
8. B. Kang and G. Ceder, *Nature*, **458**, 190 (2009).
9. Y.-T. Cheng and M. W. Verbrugge, *Journal of the Electrochemical Society*, **157**, A508 (2010).
10. Y. Saito and M. K. Rahman, *Journal of Power Sources*, **174**, 877 (2007).
11. X. Xiao, P. Liu, M. W. Verbrugge, H. Haftbaradaran, and H. Gao, *Journal of Power Sources*, **196**, 1409 (2011).
12. Y.-T. Cheng and M. W. Verbrugge, *Journal of Power Sources*, **190**, 453 (2009).
13. X. Zhang, W. Shyy, and A. M. Sastry, *Journal of the Electrochemical Society*, **154**, A910 (2007).
14. J. Christensen and J. Newman, *Journal of Solid State Electrochemistry*, **10**, 293 (2006).
15. J. Christensen and J. Newman, *Journal of the Electrochemical Society*, **153**, A1019 (2006).
16. G. Chen, X. Song, and T. J. Richardson, *Electrochemical and Solid-State Letters*, **9**, A295 (2006).
17. L. Laffont, C. Delacourt, P. Gibot, M. Y. Wu, P. Kooyman, C. Masquelier, and J. M. Tarascon, *Chemistry of Materials*, **18**, 5520 (2006).
18. C. V. Ramana, A. Mauger, F. Gendron, C. M. Julien, and K. Zaghib, *Journal of Power Sources*, **187**, 555 (2009).
19. D. A. Cogswell and M. Z. Bazant, *Acs Nano* (2012).
20. P. Bai, D. A. Cogswell, and M. Z. Bazant, *Nano Letters*, **11**, 4890 (2011).
21. A. Van der Ven, K. Garikipati, S. Kim, and M. Wagemaker, *Journal of the Electrochemical Society*, **156**, A949 (2009).
22. K. Zhao, M. Pharr, J. J. Vlassak, and Z. Suo, *Journal of Applied Physics*, **109**, 016110 (2011).
23. J. Y. Huang, L. Zhong, C. M. Wang, J. P. Sullivan, W. Xu, L. Q. Zhang, S. X. Mao, N. S. Hudak, X. H. Liu, A. Subramanian, H. Fan, L. Qi, A. Kushima, and J. Li, *Science*, **330**, 1515 (2010).
24. H. Gabrisch, J. Wilcox, and M. M. Doeff, *Electrochemical and Solid State Letters*, **11**, A25 (2008).
25. H. Wang, Y. Jang, B. Huang, D. R. Sadoway, and Y.-M. Chiang, *Journal of the Electrochemical Society*, **146**, 473 (1999).
26. H. Gabrisch, R. Yazami, and B. Fultz, *Electrochemical and Solid State Letters*, **5**, A111 (2002).
27. D. Hull and D. J. Bacon, *Introduction to dislocations* (Butterworth-Heinemann, Oxford Oxfordshire, Boston, 2001), p. 242.
28. J. Weertman, *Dislocation based fracture mechanics* (World Scientific, Singapore, River Edge, N.J., 1996) p. 524.
29. J. P. Hirth and J. Lothe, *Theory of dislocations* (McGraw-Hill, New York, 1968), p. 780.
30. J. P. Hirth, T. Mura, L. J. Teutonico, J. Dundurs, Y. T. Chou, J. C. M. Li, J. Weertman, and J. H. Weiner, *Methematical theory of dislocations* (The American Society of Mechanical Engineers, United Engineering Center, 345 East 47th Street, New York, 1969).
31. C. Delmas, M. Maccario, L. Croguennec, F. Le Cras, and F. Weill, *Nat Mater*, **7**, 665 (2008).
32. M. Broussely, P. Biensan, F. Bonhomme, P. Blanchard, S. Herreyre, K. Nechev, and R. J. Staniewicz, *Selected papers presented at the 12th International Meeting on Lithium Batteries*, **146**, 90 (2005).
33. J. Vetter, *Journal of Power Sources*, **147**, 269 (2005).
34. L. Indenbom, *Elastic strain fields and dislocation mobility*, Amsterdam; New York : Elsevier Science Publishers; New York, NY, USA : Sole distributor for the USA and Canada, Elsevier Science Pub., 1992 (1992).
35. T. Maxisch and G. Ceder, *Physical Review B*, **73**, 174112 (2006).
36. I. S. Sokolnikoff, *Mathematical Theory of Elasticity* (McGraw-Hill, New York, 1956).
37. S. P. Timoshenko and J. N. Goodier, *Theory of Elasticity* (McGraw-Hill, Inc., New York, 1970).
38. W. S. Slaughter, *The Linearized Theory of Elasticity* (Birkhauser, Boston, 2001).
39. J. F. Nye, *Physical properties of crystals, their representation by tensors and matrices* Oxford, Clarendon Press, 1957 (1957).
40. A. S. Andersson and J. O. Thomas, *Journal of Power Sources*, **97–98**, 498 (2001).
41. N. Meethong, H.-Y. S. Huang, W. C. Carter, and Y.-M. Chiang, *Electrochemical and Solid State Letters*, **10**, A134 (2007).
42. R. W. Hertzberg, *Deformation and fracture mechanics of engineering materials* (Wiley, New York, 1989).
43. A. K. Head, *Proceedings of the Physical Society of London Section B*, **66**, 793 (1953).
44. D. J. Bacon, D. M. Barnett, and R. O. Scattergood, *Progress in Materials Science*, **23**, 51 (1980).
45. X. B. Hu, Z. J. Lin, L. Liu, Y. J. Huai, and Z. H. Deng, *Journal of the Serbian Chemical Society*, **75**, 1259 (2010).
46. K.-H. Choi, J.-H. Jeon, H.-K. Park, and S.-M. Lee, *Journal of Power Sources*, **195**, 8317 (2010).
47. M. Tang, J. F. Belak, and M. R. Dorr, *Journal of Physical Chemistry C*, **115**, 4922 (2011).
48. R. Malik, F. Zhou, and G. Ceder, *Nature Materials*, **10**, 587 (2011).
49. J. L. Dodd, R. Yazami, and B. Fultz, *Electrochemical and Solid State Letters*, **9**, A151 (2006).
50. A. Yamada, H. Koizumi, S.-i. Nishimura, N. Sonoyama, R. Kanno, M. Yonemura, T. Nakamura, and Y. Kobayashi, *Nature Materials*, **5**, 360 (2006).
51. N. Meethong, H.-Y. S. Huang, S. A. Speakman, W. C. Carter, and Y.-M. Chiang, *Advanced Functional Materials*, **17**, 1115 (2007).
52. K. J. Zhao, M. Pharr, J. J. Vlassak, and Z. G. Suo, *Journal of Applied Physics*, **108** (2010).